THE SUPERCONVERGENT PATCH RECOVERY AND *A POSTERIORI* ERROR ESTIMATES. PART 1: THE RECOVERY TECHNIQUE

O. C. ZIENKIEWICZ AND J. Z. ZHU

Institute of Numerical Methods in Engineering, University College of Swansea, Singleton Park, Swansea SA2 8PP, U.K.

SUMMARY

This is the first of two papers concerning superconvergent recovery techniques and *a posteriori* error estimation. In this paper, a general recovery technique is developed for determining the derivatives (stresses) of the finite element solutions at nodes. The implementation of the recovery technique is simple and cost effective. The technique has been tested for a group of widely used linear, quadratic and cubic elements for both one and two dimensional problems. Numerical experiments demonstrate that the recovered nodal values of the derivatives with linear and cubic elements are superconvergent. One order higher accuracy is achieved by the procedure with linear and cubic elements but two order higher accuracy is achieved for the derivatives with quadratic elements. In particular, an $O(h^4)$ convergence of the nodal values of the derivatives for a quadratic triangular element is reported for the first time. The performance of the proposed technique is compared with the widely used smoothing procedure of global L_2 projection and other methods. It is found that the derivatives recovered at interelement nodes, by using L_2 projection, are also superconvergent for linear elements but not for quadratic elements. Numerical experiments on the convergence of the recovered solutions in the energy norm are also presented. Higher rates of convergence are again observed. The results presented in this part of the paper indicate clearly that a new, powerful and economical process is now available which should supersede the currently used post-processing procedures applied in most codes.

1. INTRODUCTION

The development of 'smoothing' procedures which recover more accurate nodal values of derivatives from the original finite element solution and the development of *a posteriori* error estimators which assess the accuracy of the finite element solution appear as two distinct and active areas of research in current literature. However, both are closely related, as reliable estimation of the finite element discretization error can be achieved by using an interpolation of nodally recovered values in the computations of *a posteriori* error estimators.[1] It has been shown that this type of error estimator (referred as the Zienkiewicz–Zhu or Z^2 error estimator), which uses the recovered solution in place of the exact solution in the computation of the error estimates, converges to the true error under certain conditions.[2] Recently we have shown that, if the recovery technique is superconvergent, i.e. if the recovered derivatives are superconvergent, the Zienkiewicz–Zhu error estimator will be always asymptotically exact[3,4†] in the energy norm. However, other error estimators using the maximum norm rather than the energy norm can also

___

† See also Part II of this paper

be derived by similar superconvergent recovery procedures.[3] We shall discuss in detail some of the general aspects of error estimation in Part II of this paper.

The main advantages of using the Zienkiewicz–Zhu error estimator over other types of estimators is the simplicity of its implementation and its cost effectiveness. This is due to the fact that in practical finite element computations some smoothing procedures, which may or may not be superconvergent, will always be employed in the post-processing stage of the computing process to recover the derivatives (stresses) of the finite element solutions in order to achieve more acceptable approximations. Using such recovered derivatives, the Zienkiewicz–Zhu error estimator can be calculated at a fraction of the total cost of the computation. However, the quality, and the reliability, of the error estimator is obviously dependent on the accuracy of the recovered solutions and therefore on the smoothing procedures. The requirement of higher accuracy for the recovered derivatives in the calculation of the Zienkiewicz–Zhu error estimator has led naturally to the development of the new recovery technique here presented which produces superconvergent solutions. The new recovery procedures avoid certain difficulties previously encountered for quadratic elements where a large amount of adjustment was needed to obtain reasonable results.[1]

To calculate the derivatives (stresses) from the finite element approximation, the obvious and consistent approach is that of directly differentiating the finite element solution to evaluate the resulting functions at the points of interest. For example, stresses are calculated by differentiating the displacement solution and using the appropriate constitutive relations. This direct calculation results in lower order, discontinues derivatives with inferior accuracy at the boundary of the elements and at the interelement nodes where accurate values of stresses or fluxes are usually desired. To achieve accurate derivatives the following derivative recovery techniques are currently available:

(i) *Averaging and local projection.* Nodal averaging of derivatives (or stresses) has been practised since the inception of the finite element method to present the user with more realistic results. Although the basis of the process was initially intuitive its success is closely linked with the existence of superconvergent points in many finite element solutions at which the normal rate of theoretical convergence is exceeded by one order. The existence of such *optimal sampling points* has been suggested quite early[5−7] and has been subject to much mathematical research since.[8−16] Here both quadrilateral and triangular element forms are discussed. Extrapolation from such superconvergent points and subsequent averaging at nodes (local projection) gives clearly a sound basis for improved nodal values obtainable for linear elements in which the superconvergent point is that of the element centroid for quadrilterals and that of a midside of triangles. A widely used technique of Hinton and Campbell[17] for quadrilateral quadratic elements follows a similar procedure using the 2×2 Gauss points sampling and bilinear extrapolation. For more details on such techniques a survey paper by Krizek and Neittaanmaki[18] should be consulted.

(ii) *Global projection.* A considerably more costly process of recovering accurate nodal values assumes a C_0 continuous interpolation of the derivatives of the same form as that used for the basis functions (displacements) and determines the nodal values by a least square fit to the consistently evaluated finite element solution.[19,20] Some economy can be achieved by using an iterative process,[21] but results of the method are disappointing for quadratic elements.

(iii) *Extraction and other techniques.* Other processes for determination of accurate local values by extraction, etc. exist,[22−24] and we mention these for completeness but their practical use is limited owing to excessive cost and complexity of implementation.

In the methods mentioned in (i) and (ii) above, superconvergence of the nodal derivative values is achieved only for linear elements. Indeed, in some applications the local error of the recovered solution is increased. We believe this is due to the imposition of only C_0 continuity on the global

interpolation of the derivatives. In this paper we therefore propose a new procedure in which *a single and continuous polynomial expansion of the function describing the derivatives is used on an element patch surrounding the nodes at which recovery is desired.* This expansion can be made to fit locally the superconvergent points in a least square manner or simply be an L_2 projection of the consistent finite element derivatives. The first of these processes will be shown always to lead to superconvergent recovery of nodal derivatives or stresses. The second, although not generally superconvergent, will still always result in a considerable improvement of recovered nodal values.

As both processes are *local* the cost involved in the computation is negligible and the results here presented show the very considerable improvement possible in practical calculations over currently used procedures.

The numerical tests reported here cover examples of one dimensional linear, quadratic and cubic elements; and in two dimensions linear, quadratic and cubic quadrilaterals and linear and quadratic triangles. The superconvergence of nodal values is demonstrated for the new technique, and this indeed is to be expected by the nature of the approximation.

Further, for quadratic elements of both quadrilateral and triangular types we find experimentally a convergence of $O(h^4)$ which, being two orders higher than normal, could be termed *ultraconvergence.* This result has been previously noted for some quadrilateral elements[11] but we believe that it is the first time that it has been observed for quadratic triangles. This is an important discovery as such elements have many advantages in practice, and we hope that the corresponding mathematical proof of the existence of this phenomenon can be made.

2. SUPERCONVERGENT RECOVERY PROCEDURES

In this section, we shall develop a recovery technique which uses local discrete least square smoothing and local continuous least square smoothing procedures. To illustrate the basic ideas and the implementation procedure, a linear elliptic problem of the form

$$\mathbf{Lu} \equiv \mathbf{S}^T \mathbf{DSu} = \mathbf{f} \quad \text{in } \Omega \tag{1}$$

with appropriate boundary conditions on $\partial\Omega$ is taken as the model. In the following, equation (1) may be considered as a problem of elasticity where $\mathbf{u}$ is the displacement vector, though, of course, many other problems fit into this pattern.

We shall denote by $\mathbf{u}_h$ the finite element approximation to the exact solution $\mathbf{u}$ obtained by standard Galerkin procedure,[5] and written as

$$\mathbf{u}_h = \mathbf{N\bar{u}} \tag{2}$$

The directly computed consistent, stresses, (or gradients) are

$$\boldsymbol{\sigma}_h = \mathbf{DSu}_h \tag{3}$$

where $\mathbf{\bar{u}}$ are the nodal value of the displacements, $\mathbf{N}$ are the finite element basis functions, $\mathbf{S}$ is the differential operator which defines the strain as

$$\boldsymbol{\varepsilon}_h = \mathbf{Su}_h \tag{4}$$

and $\mathbf{D}$ is the elasticity matrix.

It is well known that the stresses $\boldsymbol{\sigma}_h$ calculated from equation (3) do not possess interelement continuity and have a low accuracy at nodes and element boundaries. The objective of the recovery of the finite element derivatives is to find nodal parameters $\bar{\boldsymbol{\sigma}}^*$, such that the smoothed continuous stress field $\boldsymbol{\sigma}^*$ defined by the basis functions $\mathbf{N}$ and nodal parameters $\bar{\boldsymbol{\sigma}}^*$ as

$$\boldsymbol{\sigma}^* = \mathbf{N\bar{\sigma}}^* \tag{5}$$

is more accurate than σ_h. In the above, N are the same basis functions as the ones used for the interpolation of the displacements.

In the new recovery process we assume that the nodal values $\bar{\sigma}^*$ belong to a polynomial expansion σ_p^* of the same complete order p as that present in the basis function N and which is valid over *an element patch surrounding the particular assembly node considered*. Such a 'patch' represents a union of elements containing this vertex node (in a manner similar to that used in the patch test[5]). Illustrations of typical patches are shown in Figures 1 to 3. This polynomial expansion will be used for each component of σ_p^* (or the derivatives) and we write simply

$$\sigma_p^* = \mathbf{Pa} \tag{6}$$

where $\mathbf{P}$ contains the appropriate polynomial terms and $\mathbf{a}$ is a set of unknown parameters. For one dimensional elements of order p we can write, for instance,

$$\mathbf{P} = [1, x, x^2, \ldots, x^p] \tag{7}$$

and

$$\mathbf{a} = [a_1, a_2, a_3, \ldots, a_{p+1}]^T \tag{8}$$

In two (or three) dimensions we could similarly write only the complete polynomial terms for the appropriate element order. Thus for two dimensions and linear expansion we have

$$\mathbf{P} = [1, x, y] \tag{9}$$

and for quadratic

$$\mathbf{P} = [1, x, y, x^2, xy, y^2] \tag{10}$$

etc.

However, for quadrilaterals in which terms additional to the complete polynomial occur it appears that a slight improvement of results is obtained by using identical terms to these occurring in the shape function N. Thus for a bilinear quadrilateral we have used

$$\mathbf{P} = [1, x, y, xy] \tag{11}$$
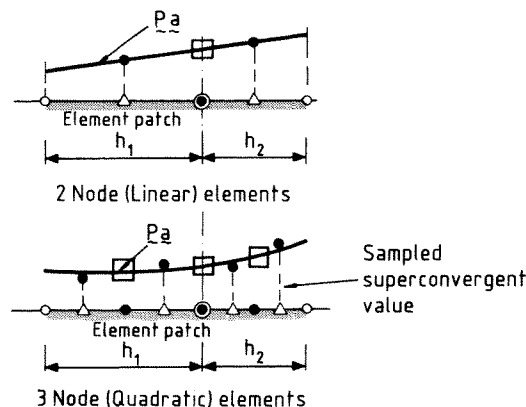
and similar forms for higher order expansions.

Figure 1. Typical element patches in one dimension showing the least square fit to sampled superconvergent Gauss point values: $\triangle$ Superconvergent Gauss point; $\square$ Nodal values determined by recovery procedure; $\odot$ 'Patch' assembly point
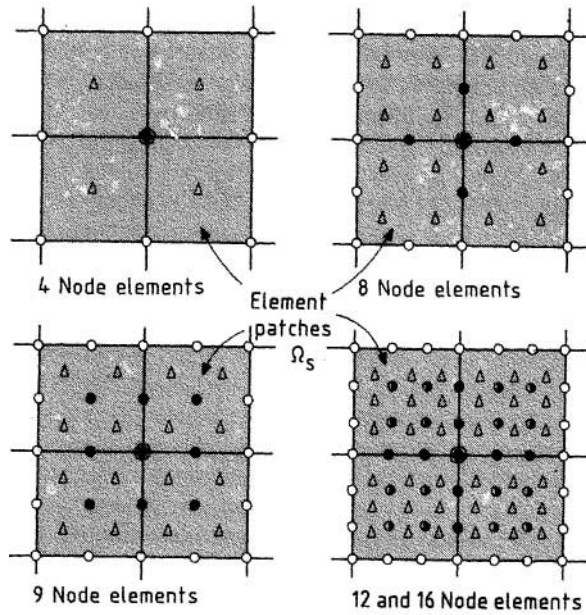
Figure 2. Computation of superconvergent nodal values for linear, quadratic and cubic quadrilateral elements: △ Gauss point; ● Nodal values determined by recovery procedure; ⊙ Patch assembly point
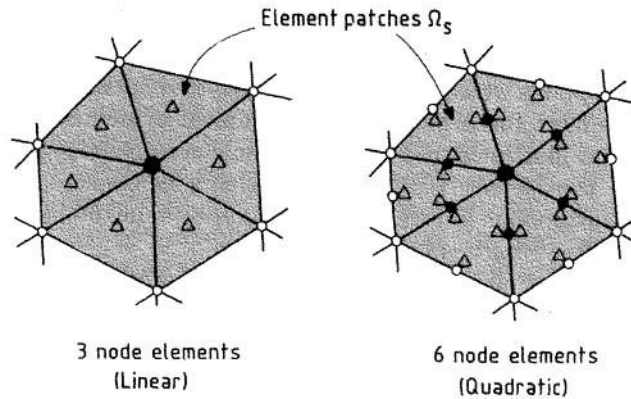
Figure 3. Computation of superconvergent nodal values for linear and quadratic triangular elements: △ Sampling point; ● Nodal values determined by recovery procedure; ⊙ Patch assembly point

2.1. Discrete superconvergent recovery in an element patch

The determination of the unknown parameters **a** of the expansion given in equation (6) is best made by ensuring a least square fit of this to the set of superconvergent or at least high accuracy sampling points existing in the patch considered if such points are available. To do this we minimize

$$F(\mathbf{a}) = \sum_{i=1}^{n} (\sigma_h(x_i, y_i) - \sigma_p^*(x_i, y_i))^2$$

$$= \sum_{i=1}^{n} (\sigma_h(x_i, y_i) - \mathbf{P}(x_i, y_i)\mathbf{a})^2 \tag{12}$$

where (x_i, y_i) are the co-ordinates of a group of sampling points, $n = mk$ is the total number of sampling points and k is the number of the sampling points on each element m_j $(m_j = 1, 2, \ldots, m)$ of the element patch $\Omega_s = \bigcup_{j=1}^{m} \Omega_{m_j}$ (see Figures 1 to 3).

The minimization condition of $F(\mathbf{a})$ implies that $\mathbf{a}$ satisfies

$$\sum_{i=1}^{n} \mathbf{P}^T(x_i, y_i)\mathbf{P}(x_i, y_i)\mathbf{a} = \sum_{i=1}^{n} \mathbf{P}^T(x_i, y_i)\sigma_h(x_i, y_i) \tag{13}$$

This can be solved in matrix form as

$$\mathbf{a} = \mathbf{A}^{-1}\mathbf{b} \tag{14}$$

where

$$\mathbf{A} = \sum_{i=1}^{n} \mathbf{P}^T(x_i, y_i)\mathbf{P}(x_i, y_i) \quad \text{and} \quad \mathbf{b} = \sum_{i=1}^{n} \mathbf{P}^T(x_i, y_i)\sigma_h(x_i, y_i) \tag{15}$$

The number of equations to be solved on each patch is modest and the recovery is performed only for each vertex node. The procedure is therefore quite inexpensive. We note in passing that precisely the matrix same $\mathbf{A}$ occurs in the solution for each component of $\boldsymbol{\sigma}_p^*$ and hence only a single evaluation of this is necessary.

Once the parameters $\mathbf{a}$ are determined the recovered nodal values of $\bar{\boldsymbol{\sigma}}^*$ are simply calculated by insertion of appropriate co-ordinates into the expression for $\boldsymbol{\sigma}_p^*$. Here only the nodes *inside* of the patch are considered, as shown in Figures 1 to 3.

It can be expected that all values of $\boldsymbol{\sigma}_p^*$ in the domain of the patch are superconvergent as it fits closely to local sampling points which exhibit this property and is also of the correct polynomial order. As we shall show later, this argument is substantiated by numerical results.

The procedure is simply illustrated on a one dimensional example of Figure 1 where linear and quadratic elements are considered. It is well known that superconvergence of the derivatives occurs here at the Gauss points shown,[11] and the appropriate fit of linear and quadratic polynomials over an element patch is indicated.

In Figure 2 we show the sampling points for patches of quadrilateral elements with $p = 1$ to 3. Here again the derivatives at appropriate Gauss points are known to be superconvergent.[8-11] Obviously the procedure could be used for any order of p for such elements.

In Figure 3 a similar procedure is applied to triangular elements of linear and quadratic types. For triangular shapes the existence and the locations of superconvergent points are still a matter which does not appear to have been fully explored mathematically despite the early work of Moan suggesting the existence of optimal integration points.[6] In the linear form the average of the derivative values at mid sides of adjacent elements is proved superconvergent.[12,13] For practical purposes, however, this is equivalent to stating that the centroidal point value of the element is superconvergent, and we have here used this as the basis, though this is not rigorously correct. For quadratic triangles no fully superconvergent points appear to be known though it is suggested that some of the derivatives (those parallel to the sides) are superconvergent at two side Gauss points.[14,15] Here we use a simpler but purely experimental finding that the central values at sides are *optimal* (see Figure 3) and we find an extraordinary fact that the resulting recovered values at nodes are 'ultraconvergent' i.e. with order of $O(h^4)$.

We have not yet investigated higher order triangles with $p \geq 3$, and here further work remains to be done.

2.2. An alternative local L_2 projection recovery in an element patch

It is well known[5] that in self-adjoint problems of the type here discussed the values of σ_h are a global least square fit to the exact solution. The local polynomial solution could thus be obtained over the element patch by ensuring that it minimizes for each component

$$F(\mathbf{a}) = \int_{\Omega_s} (\sigma_h - \sigma_p^*)^2 \, d\Omega$$

$$= \int_{\Omega_s} (\sigma_h - \mathbf{Pa})^2 \, d\Omega \tag{16}$$

where $\Omega_s = \bigcup_{j=1}^{m} \Omega_{m_j}$ is the domain of the element patch previously discussed.

The minimization condition of $F(\mathbf{a})$ results in

$$\int_{\Omega_s} \mathbf{P}^T \mathbf{P} \, d\Omega \mathbf{a} = \int_{\Omega_s} \mathbf{P}^T \sigma_h \, d\Omega \tag{17}$$

In matrix form, this can be written again as

$$\mathbf{a} = \mathbf{A}^{-1} \mathbf{b} \tag{18}$$

with

$$\mathbf{A} = \int_{\Omega_s} \mathbf{P}^T \mathbf{P} \, d\Omega \quad \text{and} \quad \mathbf{b} = \int_{\Omega_s} \mathbf{P}^T \sigma_h \, d\Omega \tag{19}$$

The order of matrix $\mathbf{A}$ is clearly the same as the number of the terms of the polynomial used in $\mathbf{P}$.

If the integration is carried out numerically for matrices of equation (19) then expressions will become similar to those of equation (15) with each term of the summation multiplied now by an appropriate weighting coefficient and element area. Indeed if *reduced* integration corresponding to the superconvergent points of the previous section is used then identical results will be obtained with those of the previous section for regular assemblies of, the *linear* and *quadratic* *elements* for which all the weightings are the same. This, however, does not carry over to elements higher than the quadratic form and identity is lost when more accurate integration is used.

Indeed, we find in the numerical tests that the above form (corresponding to an L_2 projection over the element patch) does not result in superconvergence of nodal values for quadratic elements though considerable improvement of these values is noted.

We have nevertheless observed an interesting fact. If the local fit of the polynomial in Section 2.1 is made to Gauss point values with a number greater than that necessary for superconvergence (say 3×3 for quadratic quadrilaterals) then at least equally good and superconvergent results are still obtained even though this does not fully correspond to an integration. This phenomenon is not easy to explain and further investigations are in progress.

2.3. Interelement and boundary nodes

It will be observed from the preceding that element patches will overlap for internal midside nodes and nodes in the element interior. This means that such recovered nodal values are frequently evaluated from two patches. As all such values are superconvergent: if the procedure of Section 2.1 is used we recommend that an average value is used for such nodes. The recovered assembly (vertex) nodal values are, however, only determined from a single patch.

A more difficult situation arises at the domain boundary where a local patch, such as we illustrate in Figure 4, may involve only one or two elements. For the one element situation (corner node) the size of the patch is insufficient for determination of the parameters **a** and the corner node values are determined from an interior patch shown. For two element patches the situation is simpler and such patches are assembled and solved in the standard manner as shown. However, all the boundary nodes values can be determined by interior patches instead of boundary patches and the results are equally accurate. We therefore recommend this as a general procedure.

The recovered boundary nodal values are still superconvergent but now for quadratic elements the ultraconvergence of $O(h^4)$ will not be present.

3. NUMERICAL STUDIES

In this section we report numerical studies on several problems for which exact solutions are available to demonstrate the accuracy of the recovered derivatives achieved by the proposed recovery procedures and their rates of convergence. The test include one and two dimensional problems with various element shapes used in the latter. The results of σ^* presented in this paper are computed by the discrete recovery procedure of Section 2.1. We shall give a full report of the numerical tests on the recovery procedure of the local L_2 projection of Section 2.2 elsewhere.

Only regular subdivision can of course be used to study the convergence rates but the accuracy of the solutions is also demonstrated for some irregular meshes.

Comparisons are carried out for some alternative recovery procedures. In particular we shall show results obtained by the global L_2 projections[19,20] using the iterative process of solving the equation.[21] We denote such results by superscript L, i.e. σ^L.

For quadratic quadrilaterals we shall also assess the widely used local projection procedure of Hinton and Campbell[17] and label the results with the superscript HC, i.e. σ^{HC}.

The results will be given, in Section 3.1 and Section 3.2, for the convergence of the recovered nodal values and in Section 3.3 for the convergence of the recovered solution in the energy norm. The examples presented in Sections 3.1 to 3.2 are for one and two dimensional self-adjoint problems with a scalar variable. In Section 3.4 we shall examine the convergence of the recovered nodal stress values for an elastic problem. To provide a record the Appendix presents some results in a tabular form, in addition to the figures illustrating in this paper.

A difficulty occurs in reporting the nodal σ_h, as the consistent finite element values are multivalued because of discontinuity. We have chosen therefore the value giving the maximum absolute error unless otherwise specified.
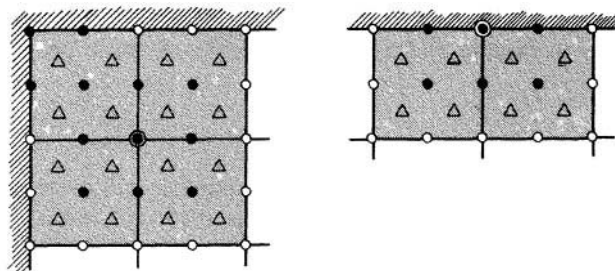

Figure 4. Boundary nodal recovery. Element patches: △ Sampling point; ● Nodal values determined by recovery procedure; ⊙ Patch assembly point

3.1. The convergence of nodal values: One dimensional problems

Example 1. As a test problem we take the equation

$$-\frac{d}{dx}\left(\frac{du}{dx}\right) + u = f \quad \text{on } I = (0, 1) \tag{20}$$

with boundary conditions

$$u(0) = 0 \quad \text{and} \quad u(1) = 0 \tag{21}$$

The function f is chosen so that the exact solution is of the form

$$u = x^2 - \frac{\text{sh } 4x}{\text{sh } 4} \tag{22}$$

where sh is the hyperbolic sine function and we define

$$\sigma = \frac{du}{dx} \tag{23}$$

A sequence of uniform refinements is employed in the finite element analysis using linear, quadratic and cubic elements.

Pointwise errors of σ_h, σ^L and σ^* are examined at an interelement point $x = 0.5$. σ_h, which is discontinuous, is calculated by differentiating the finite element solution from the element containing this point and on which $x \geqslant 0.5$. Numerical results of using linear, quadratic and cubic elements are presented in Figures 5(a), 5(b) and 5(c), in log scale, to demonstrate the convergence of σ_h, σ^L and σ^*. These results are also presented in Tables I(a), I(b) and I(c) respectively in the Appendix.
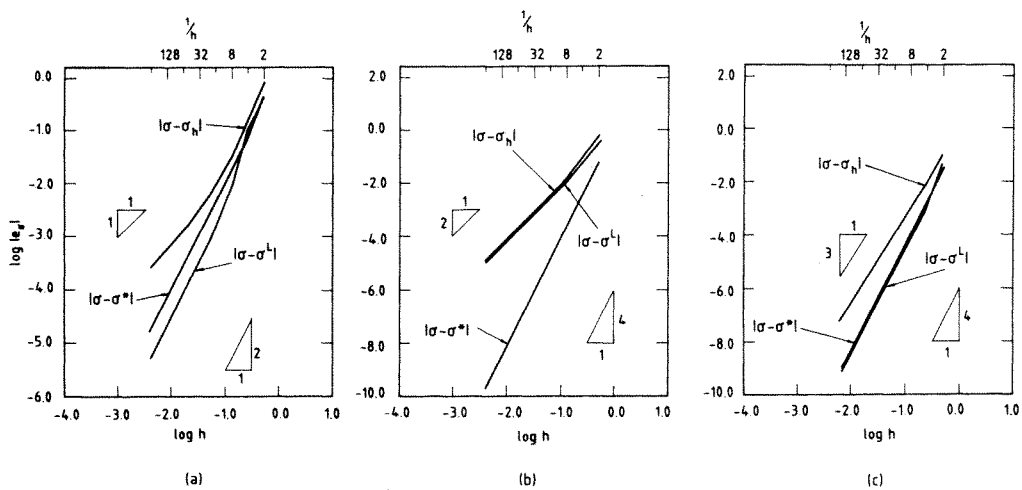
Figure 5. Rate of convergence of σ_h, σ^L and σ^* at $x = 0.5$. One dimensional problem of Example 1: (a) Linear element; (b) Quadratic element; (c) Cubic element

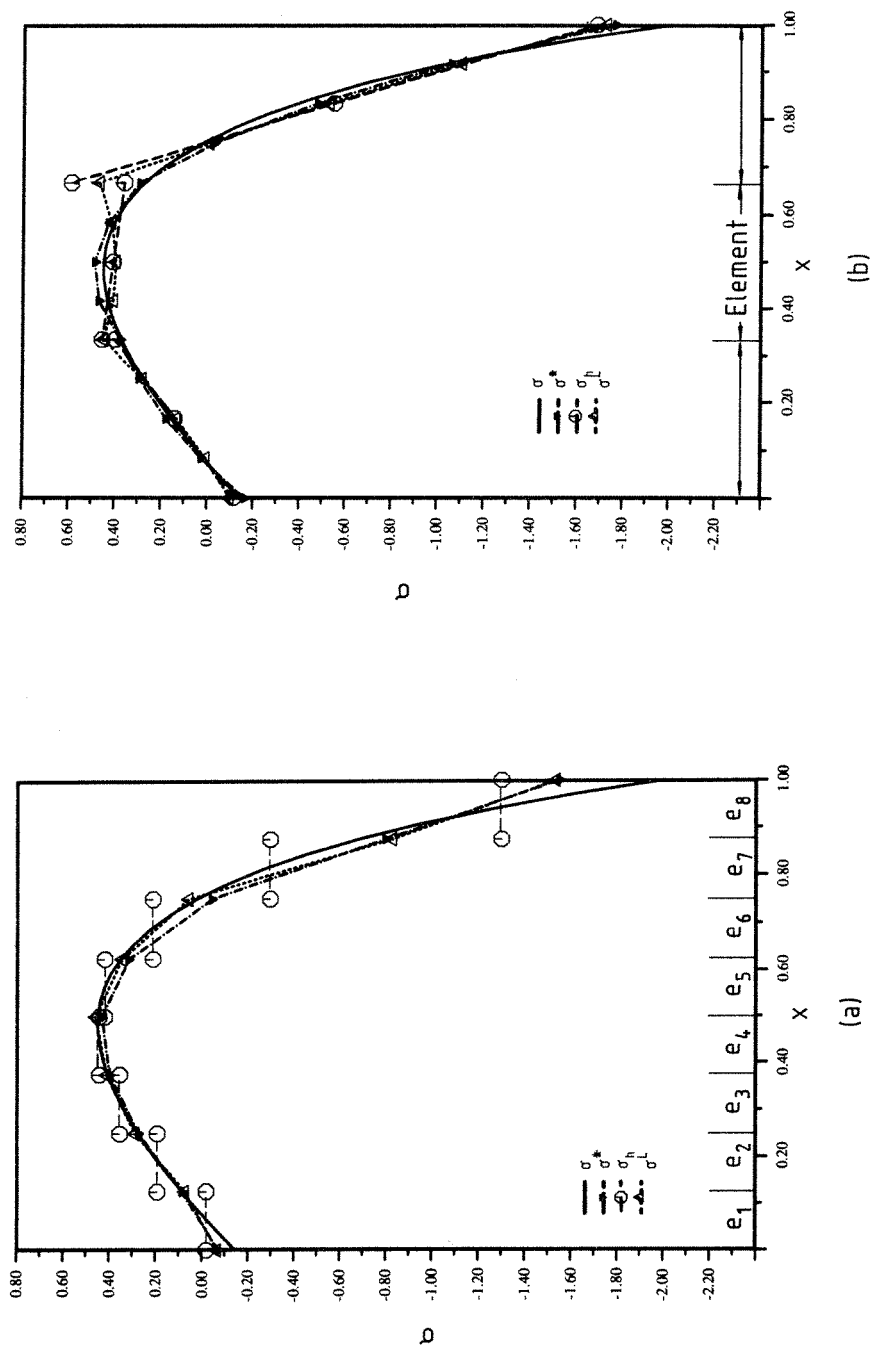Figure 6. Distribution of the exact solution σ, finite element solution of σ_h and recovered solutions σ^* and σ^L in problem of Example 1: (a) Linear elements; (b) Quadratic elements

We observe, from the results, that:

(i) σ_h exhibits $O(h^P)$ convergence as predicted by *a priori* error estimation;

(ii) the interelement nodal value of σ^L is superconvergent for linear and cubic elements with $O(h^{P+1})$ convergence, but not superconvergent for the quadratic element as only $O(h^P)$ convergence occurs. Indeed, the difference between σ^L and σ_h is small for the quadratic element, with this difference decreasing as the mesh is refined;

(iii) σ^* is superconvergent for all three elements. It shows $O(h^{P+1})$ convergence for linear and cubic elements and $O(h^{P+2})$ convergence for the quadratic element;

(iv) for linear and cubic elements, the recovered interelement nodal values of σ^L are slightly more accurate than those of σ^*, though both of them are superconvergent.

The values of σ_h, σ^L and σ^* together with the exact solution σ over the whole domain of I are plotted in Figure 6(a) for eight linear elements and in Figure 6(b) for three quadratic elements. The following remarks can be made by observing Figure 6.

(i) It is well known that for linear elements the derivative of the finite element solution has the biggest local error at interelement nodes where it is discontinuous (as shown in Figure 6(a)). This turns out to be also true for the quadratic elements (see Figure 6(b)).

(ii) The recovered derivative nodal values σ^L and σ^* for linear elements are located between the discontinuity of the finite element solution σ_h. These values are superconvergent, as we have shown. For quadratic elements, the interelement nodal value of σ^L is again located between the discontinuity of σ_h. It is, however, not superconvergent. This implies that a simple average of the discontinuous derivative values of the finite element solution will not result in superconvergent nodal values for quadratic elements as it does for linear elements.

The convergence of the nodal values of σ_h, σ^L and σ^* at the boundary of the domain $x = 1 \cdot 0$, which are computed from an interior patch, are also examined and illustrated in Figures 7(a), 7(b) and 7(c). It is observed that the boundary values of σ^L have only the standard rate of convergence
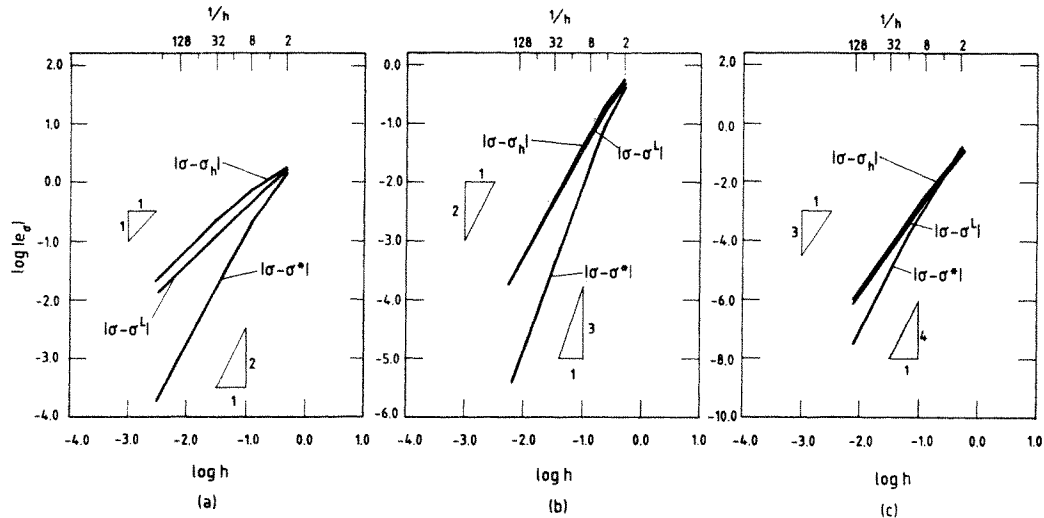

Figure 7. Rate of convergence of σ_h, σ^L and σ^* at boundary $x = 1 \cdot 0$. Example 1: (a) Linear element; (b) Quadratic element; (c) Cubic element

$O(h^p)$. The superconvergence of σ^L at interelement nodes disappears at the boundary. In fact, the difference between σ^L and σ_h at the boundary is small though σ^L is slightly more accurate. The σ^* is still superconvergent at the boundary; however, its convergence rate for quadratic elements is reduced from $O(h^{p+2})$ to $O(h^{p+1})$.

From what we have stated above based on results of a test problem with equal elements, it would appear that the new method of recovery is not significantly better for linear elements than the currently used L_2 projection or simple averaging (except at boundary nodes). However its advantage is very large when unequal size elements are used. We show this in Figure 8—on which both L_2 and simple averaging are contrasted with the new process.

This figure demonstrates that here only the new process tends to the exact solution at all points. . . . It also shows that simple averaging is better here than the L_2 projection.

3.2. The convergence of nodal values: Two dimensional problems

The following model problem is considered to test the recovery procedure for two dimensional linear and quadratic elements. Equally accurate and for a general code we recommend exclusive use of this procedure.

Example 2. The governing equation is

$$-\Delta u = f \quad \text{in } \Omega \tag{24}$$

with boundary condition
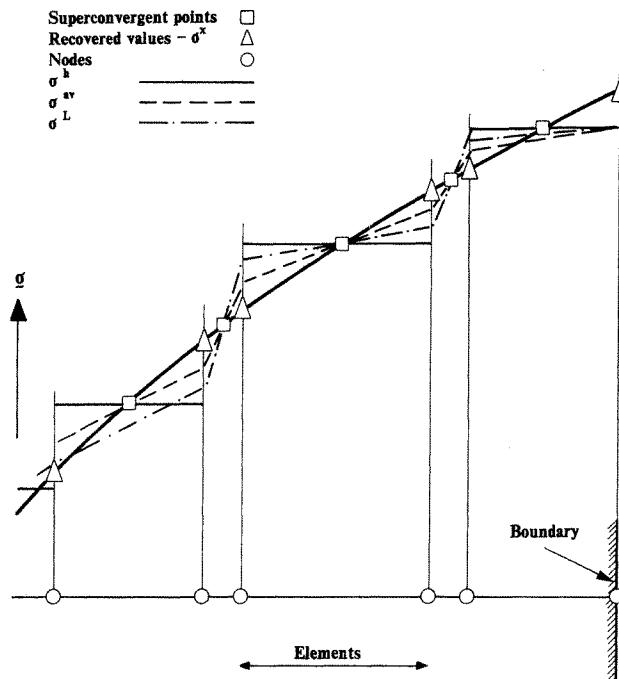
$$u = 0 \quad \text{on } \partial\Omega \tag{25}$$

Figure 8. Performance of the new recovery process *vs* L_2 and averaging for unequal size, linear elements

where Ω is a unit square domain $\Omega = (0, 1) \times (0, 1)$ and f is constructed to correspond to the exact solution

$$u(x, y) = x(1 - x)y(1 - y)(1 + 2x + 7y) \tag{26}$$

This problem has been used by Zlamal[8] and Lesaint and Zlamal[9] to demonstrate the superconvergence of the derivatives at Gauss points for eight node quadratic (Serendipity) elements.

Here we define

$$\boldsymbol{\sigma} = \nabla u \tag{27}$$

with

$$\sigma_x = \frac{\partial u}{\partial x} \quad \text{and} \quad \sigma_y = \frac{\partial u}{\partial y} \tag{28}$$

The local error of the recovered derivatives $\boldsymbol{\sigma}^L$, $\boldsymbol{\sigma}^*$ and $\boldsymbol{\sigma}^{HC}$ is fully examined at a vertex nodal point with co-ordinates of $(0.25, 0.25)$ where the exact solution has the values of $\sigma_x = 0.375$ and $\sigma_y = 0.55078125$. Uniform subdivisions are used in the finite element analysis for both quadrilateral and triangular elements.

While a vertex nodal point will remain as the vertex point during the mesh subdivision the same is not true for nodes located on element faces. To study the convergence of the recovered derivatives at midside nodes, for instance, we shall examine the errors at the nearest midpoint to the above vertex point of the subdivision. For quadratic quadrilateral elements we shall also report the convergence of the recovered solution at a boundary point.

3.2.1. Linear and quadratic quadrilateral elements.

The numerical results of the convergence of the recovered derivatives for a 4 node bilinear element are plotted in Figure 9(a). It is observed that both σ_x^L, σ_y^L and σ_x^*, σ_y^* are superconvergent with $O(h^2)$, i.e. $O(h^{p+1})$, convergence as found for one dimensional linear element. Four terms of polynomial are used in the recovery procedure, though a three term polynomial will provide similar results. The above results of σ_x^L and σ_x^* are also presented in Table II in the Appendix.

For the 8 node Serendipity element, the results of $\boldsymbol{\sigma}^{HC}$ and $\boldsymbol{\sigma}^*$ are presented in Figure 9(b). The computation of global L_2 projection for this type of element is expensive and therefore not included in the present study. We observe, in Figure 9, that σ_x^* and σ_y^* are superconvergent with $O(h^4)$, i.e. $O(h^{p+2})$. This is the same convergence rate as that found for the one dimensional quadratic element (eight terms of polynomial are here used in the smoothing function although essentially the same results are achieved with a six term polynomial). It is also noted that the results of $\boldsymbol{\sigma}^{HC}$ exhibit only standard convergence of $O(h^2)$, i.e. $O(h^p)$, and that $\boldsymbol{\sigma}^*$ is much more accurate than $\boldsymbol{\sigma}^{HC}$. The above results of σ_x^{HC} and σ_x^* can also be found in Table III in the Appendix.

The convergence of the recovered derivatives $\boldsymbol{\sigma}^L$, $\boldsymbol{\sigma}^*$ and $\boldsymbol{\sigma}^{HC}$ is illustrated for a 9 node biquadratic element in Figure 10. An eight term polynomial is again used in the smoothing function. It is found, from Figure 10(a) for the vertex node and Figure 10(b) for the midside node, that σ_x^* and σ_y^* are both again superconvergent as they are for an 8 node element with $O(h^4)$ convergence. It is also observed, from Figure 10(c), that for a boundary node with co-ordinates of $(0.75, 1.0)$ σ_y^* is still superconvergent with $O(h^4)$, but σ_x^* is superconvergent with a reduced rate of $O(h^3)$. However, σ_x^L and σ_y^L have only standard convergence of $O(h^2)$, just as is the case with σ_h. This again appears to be the case with the results of the Hinton–Campbell extrapolation $\boldsymbol{\sigma}^{HC}$. Indeed, neither set gives significantly better results than $\boldsymbol{\sigma}_h$. The results of σ_x^L, σ_x^{HC} and σ_x^* for the vertex node are also presented in Table IV in the Appendix.
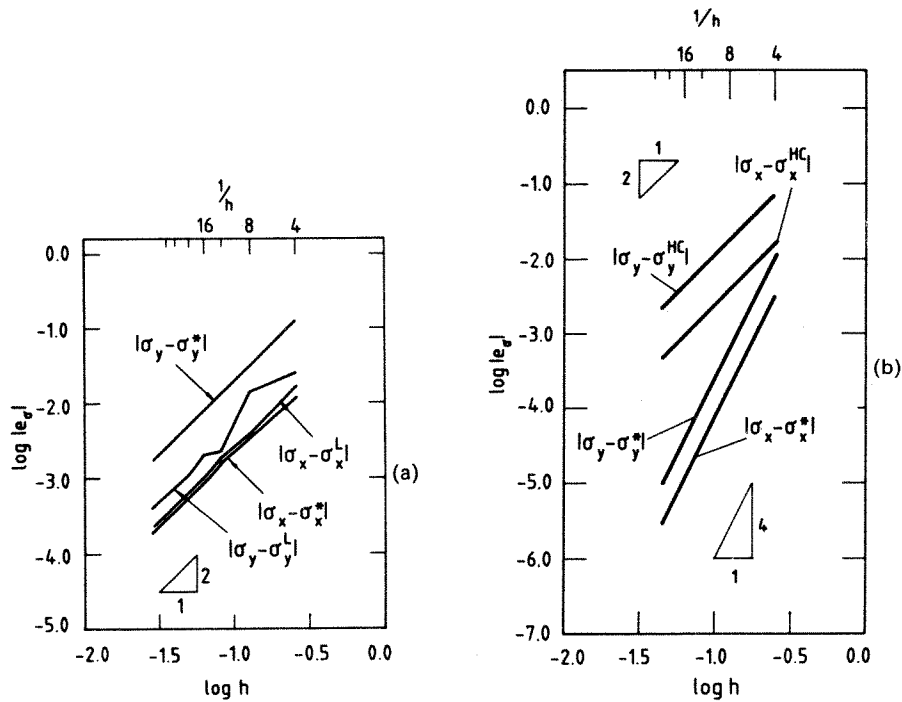
Figure 9. Problem of Example 2 rate of convergence of errors in $\sigma^*\sigma^L$ and σ^{HC} at the point (0·25, 0·25) (a) 4 node linear element. (b) 8 node quadratic (Serendipity) element
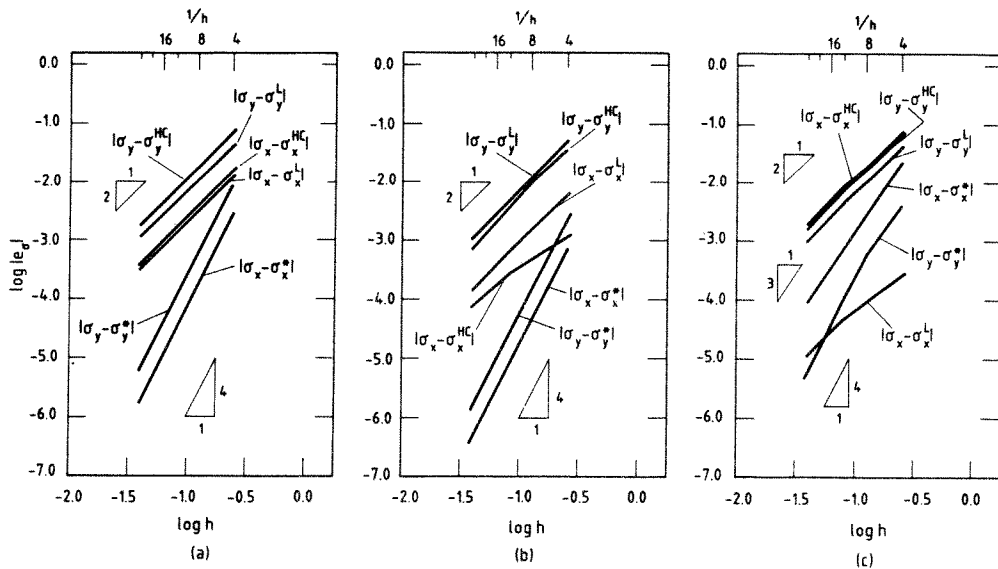
Figure 10. Rate of convergence of σ^*, σ^L and σ^{HC} for the biquadratic two dimensional problem of Example 2: (a) Point (0·25, 0·25)—Corner node; (b) Point near (0·25, 0·25)—Midside node; (c) Point (0·75, 1·00)—Boundary point

Remark. In the study of the superconvergence of the derivatives at Gauss points for an 8 node element, Zlamal[8] pointed out that, to calculate the nodal values of the derivatives, interpolation from four Gauss points on each element by a linear isoparametric shape function would make worse the accuracy won by superconvergence. A local interpolation procedure was proposed by him, which interpolates the $O(h^{p+1})$ superconvergent Gauss point derivative values to the nodal points. The procedure, however, needs to solve a non-linear equation. Comparatively, the smoothing procedure discussed in this paper is much simpler and indeed provides the recovered derivatives at nodes with an ultraconvergence of the order $O(h^{p+2})$.

The preceding discussion on convergence rates has perforce concentrated on a limited number of nodal values. To appreciate the overall accuracy of the recovery procedure we plot the distribution of nodal errors as contours over the complete domain for a given subdivision. Such contours are plotted in Figure 11 using regular 12×12 subdivision for errors in σ_h, σ^L, σ^{HC} and σ^*. The very significant improvement of the error given by the new procedure over the previous recovery methods must be noted.

In Figure 12 a similar set of contours is given for a completely irregular mesh.

It is also interesting to observe from Figures 11 and 12 that the global L_2 projection is more effective on the irregular mesh, i.e. the error of σ^L is much smaller than that of σ_h. The error of σ^{HC} is, however, larger than that of σ_h on both regular and irregular meshes.

3.2.2. Linear and quadratic triangular elements. Linear triangular elements are now employed in solving Example 2 using again regular meshes.
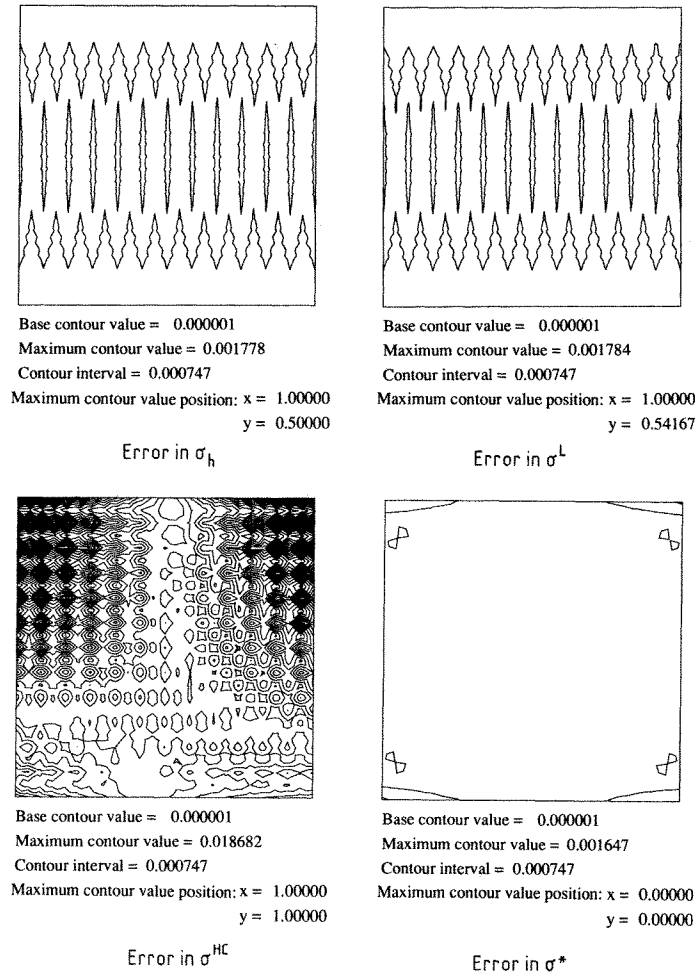
The numerical results of the convergence of the recovered derivative nodal values at point $(0.25, 0.25)$ for a 3 node linear triangular element are presented in Figure 13(a) to demonstrate the rate of convergence of the recovered solutions. Three terms of the polynomial are used in the recovery procedure. It is found that both σ_x^L, σ_y^L and σ_x^*, σ_y^* are superconvergent with convergence of $O(h^2)$ and that the results given by global L_2 projection seem to be more accurate. The results of σ_x^L and σ_x^* are also given in Table V in the Appendix.

The problem is also analysed by using 6 node quadratic triangular elements. It is observed, from Figure 13(b), that the convergence of σ_x^L and σ_y^L has the standard rate of $O(h^2)$. However, σ_x^* and σ_y^* show ultraconvergence with order of $O(h^4)$, just as that achieved for quadratic quadrilateral elements. The numerical results of σ_x^L and σ_x^* are also presented in Table VI in the Appendix.

Remark. No superconvergence of order $O(h^4)$ for the derivative of a quadratic triangular element has been reported before by any recovery technique. In fact, although different techniques have been developed to recover superconvergent derivatives for linear triangular elements, the only technique proposed for recovering superconvergent derivatives for a quadratic triangular element is averaging at the two Gauss points of each side of the quadratic triangular elements.[14,15] This technique proves superconvergence of the tangential component of the derivatives with the rate of convergence of $O(h^3)$. The procedure used to extend this result to the superconvergence of the full gradients at the vertices of the elements is complicated and not practical. The technique proposed in this paper is, up to now, the only recovery technique which can produce superconvergence of gradients for a quadratic triangular element and with superconvergence order of $O(h^4)$.

The discovery of the possible $O(h^4)$ superconvergence for quadratic triangular elements is also encouraging to those who prefer to use triangular elements and also wish to achieve high accuracy economically.

3.2.3. Cubic quadrilateral elements. To examine the accuracy of the recovered derivatives for cubic elements, we shall consider the following model problem.

Base contour value = 0.000001
Maximum contour value = 0.001778
Contour interval = 0.000747
Maximum contour value position: x = 1.00000
                                 y = 0.50000

Error in σ_h

Base contour value = 0.000001
Maximum contour value = 0.001784
Contour interval = 0.000747
Maximum contour value position: x = 1.00000
                                 y = 0.54167

Error in σ^L

Base contour value = 0.000001
Maximum contour value = 0.018682
Contour interval = 0.000747
Maximum contour value position: x = 1.00000
                                 y = 1.00000

Error in σ^{HC}

Base contour value = 0.000001
Maximum contour value = 0.001647
Contour interval = 0.000747
Maximum contour value position: x = 0.00000
                                 y = 0.00000

Error in σ^*

Figure 11(a). Contours of σ_x nodal error distribution. Regular 12×12 mesh, 9 node element. Example 2

Example 3.

$$-\Delta u = f \quad \text{in } \Omega \tag{29}$$

and

$$u = \bar{u} \quad \text{on } \partial\Omega \tag{30}$$

where Ω is a unit square $\Omega = (0, 1) \times (0, 1)$ and f is chosen such that the exact solution is of the form

$$u(x, y) = 1 + xy + \text{sh}(4x + 4y) \tag{31}$$

A sequence of uniform subdivisions of the domain Ω is again used in the analysis. The local error of σ^* is examined at node point $(0.75, 0.75)$ where $\sigma_x = \sigma_y$ and the exact solution is $\sigma_x = 0.80761254E + 03$.

The numerical results of σ_x^* for a 12 node element with 13 terms of the polynomial used in the smoothing function and a 16 node element with 15 terms of the polynomial used in the smoothing function are illustrated in Figure 14. We observe that the superconvergence of σ^* with $O(h^4)$
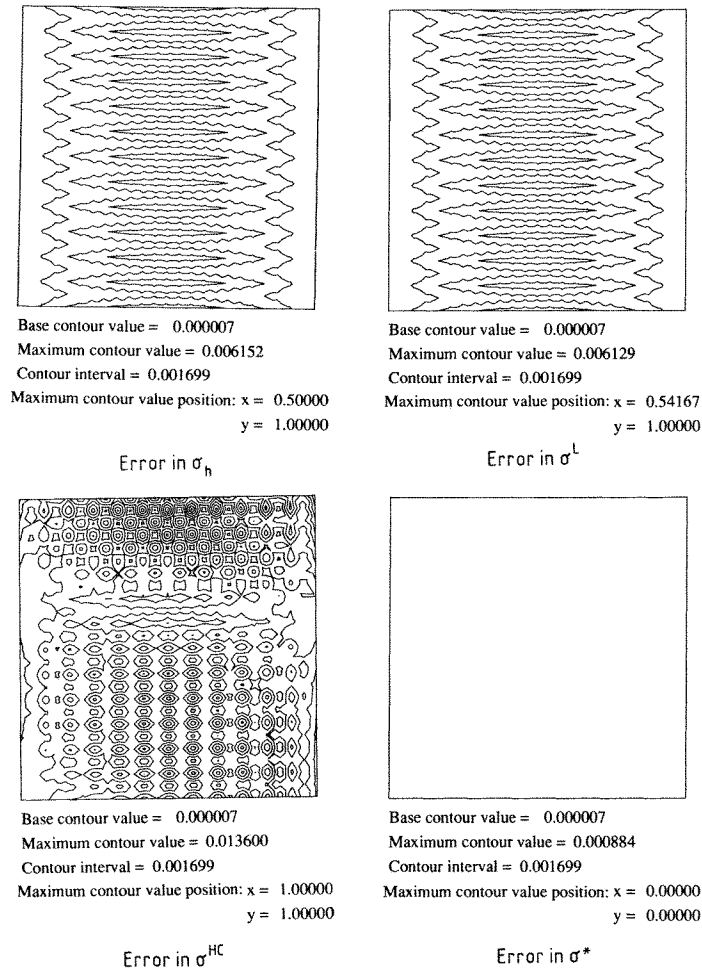
Base contour value =   0.000007
Maximum contour value = 0.006152
Contour interval = 0.001699
Maximum contour value position: x =   0.50000
                                                  y =   1.00000

Error in σ_h

Base contour value =   0.000007
Maximum contour value = 0.006129
Contour interval = 0.001699
Maximum contour value position: x =   0.54167
                                                  y =   1.00000

Error in σ^L

Base contour value =   0.000007
Maximum contour value = 0.013600
Contour interval = 0.001699
Maximum contour value position: x =   1.00000
                                                  y =   1.00000

Error in σ^{HC}

Base contour value =   0.000007
Maximum contour value = 0.000884
Contour interval = 0.001699
Maximum contour value position: x =   0.00000
                                                  y =   0.00000

Error in σ^*

Figure 11(b). Contours of σ_y nodal error distribution. Regular 12×12 mesh, 9 node element. Example 2

convergence is achieved for both 12 and 16 node elements (it is one order higher than the standard convergence of $O(h^3)$). These results are also illustrated in Tables VII and VIII respectively in the Appendix.

3.3. The convergence of the recovered solutions in energy norm

We shall in the following examine the convergence of the recovered solutions as well as the finite element solution in the energy norm. While computing the error of the recovered solutions only the derivative terms appearing in the energy norm are considered. The basic function term, which should be included in the energy norm for problems such as equation (20) of Example 1, is omitted because it is not available from the recovery procedures discussed in this paper. However, the error in the basic function term is of higher order; its omission therefore will not affect the rate of convergence which is the main concern of our study.
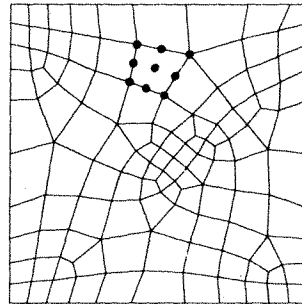
Figure 12(a). Nodal error distribution for an irregular mesh of 9 node elements. Example 2
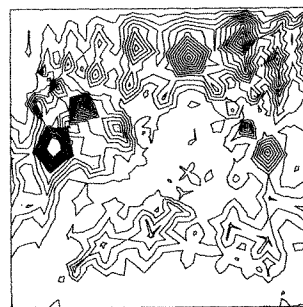
Base contour value = 0.000002

Maximum contour value = 0.047780

Contour interval = 0.002436

Maximum contour value position: x = 0.14893

y = 0.53928
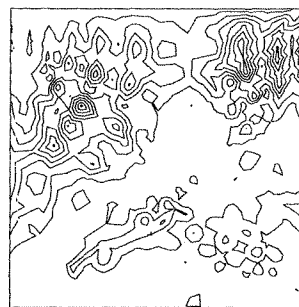
Error in σ_h

Base contour value = 0.000002

Maximum contour value = 0.021198

Contour interval = 0.002436

Maximum contour value position: x = 1.00000

y = 0.86794

Error in σ^L
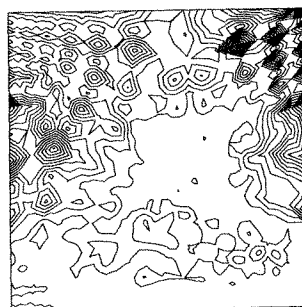
Base contour value = 0.000002

Maximum contour value = 0.036540

Contour interval = 0.002436

Maximum contour value position: x = 1.00000

y = 0.68068

Error in σ^{HC}

Base contour value = 0.000002

Maximum contour value = 0.008361

Contour interval = 0.002436

Maximum contour value position: x = 1.00000

y = 1.00000

Error in σ^*

Figure 12(b). σ_x nodal error distribution

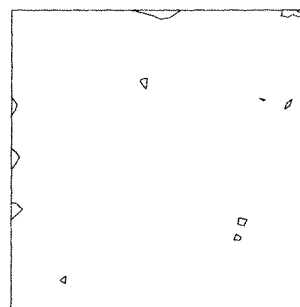Base contour value = 0.000003
Maximum contour value = 0.029747
Contour interval = 0.003661
Maximum contour value position: x = 0.14893
y = 0.53928

Error in σ_h

Base contour value = 0.000003
Maximum contour value = 0.027419
Contour interval = 0.003661
Maximum contour value position: x = 0.94066
y = 1.00000

Error in σ^L

Base contour value = 0.000003
Maximum contour value = 0.057912
Contour interval = 0.003661
Maximum contour value position: x = 0.79973
y = 1.00000

Error in σ^{HC}

Base contour value = 0.000003
Maximum contour value = 0.005759
Contour interval = 0.003661
Maximum contour value position: x = 0.79973
y = 1.00000

Error in σ^*

Figure 12(c). σ_y nodal error distribution

Example 1 will be again considered in the study of one dimensional elements and Example 2 will be used for examining the two dimensional elements.

For Example 1, the error of the finite element solution in the energy norm is written as

$$\| e \| = \| u - u_h \| = \left\{ \int_I ((\sigma - \sigma_h)^2 + (u - u_h)^2) \, \mathrm{d}x \right\}^{1/2} \tag{32}$$

and the error of the recovered solution in the energy norm is written as

$$\| e^R \| = \| u - u^R \| = \left\{ \int_I (\sigma - \sigma^R)^2 \, \mathrm{d}x \right\}^{1/2} \tag{33}$$

where superscript R represents the recovery procedure and will be replaced by L and *.

Figure 13. Rate of convergence of σ^L and σ^* at (0·25, 0·25). Two dimensional problem of Example 2: (a) Linear 3 node triangle; (b) Quadratic 6 node triangle

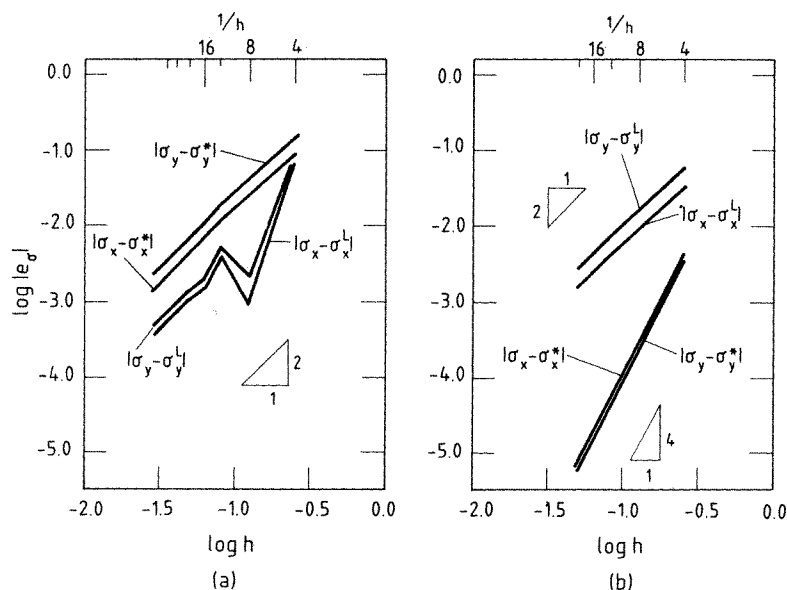For Example 2, the error of the finite element solution in the energy norm is written as

$$\| e \| = \| u - u_h \| = \left\{ \int_\Omega (\sigma - \sigma_h)^T (\sigma - \sigma_h) \, d\Omega \right\}^{1/2} \tag{34}$$

and similarly for the recovered solution we have

$$\| e^R \| = \| u - u^R \| = \left\{ \int_\Omega (\sigma - \sigma^R)^T (\sigma - \sigma^R) \, d\Omega \right\}^{1/2} \tag{35}$$

here again superscript R will be replaced by L, HC and *.

3.3.1. Numerical experiments for one dimensional elements. The numerical results of the convergence of the recovered solutions and the finite element solution in the energy norm are plotted in Figures 15(a), 15(b) and 15(c) for linear, quadratic and cubic elements respectively. These results are also presented in Tables IX(a), IX(b) and IX(c) in the Appendix. From Figure 15 and Table IX the following are observed:

  (i) $\| e \|$, as predicted, has standard $O(h^p)$ convergence;
 (ii) $\| e^L \|$ has a higher convergence rate of $O(h^{1·5})$, i.e. $O(h^{p+0·5})$, than the standard rate $O(h)$ for linear elements, but exhibits only standard convergence for quadratic and cubic elements;
(iii) $\| e^* \|$ is superconvergent. It has a convergence rate of $O(h^{p+1})$ for all linear, quadratic and cubic elements.

By comparing the corresponding figures of Figures 5, 7 and 15, it is found that the convergence of the recovered solutions in the energy norm is strongly affected by the convergence of the
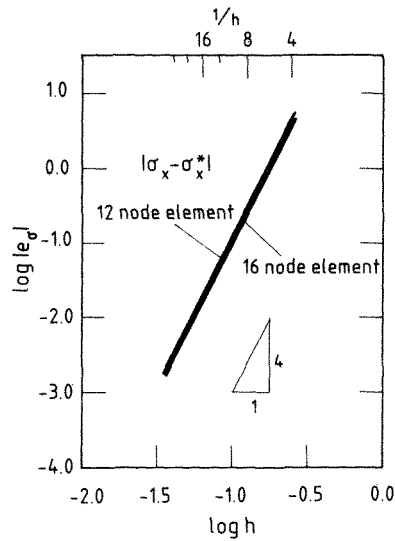
Figure 14. Rate of convergence of σ^* ($\sigma_x^* = \sigma_y^*$) for a two dimensional problem of Example 3. 12 node and 16 node cubic elements. Results shown for (0·75, 0·75) point
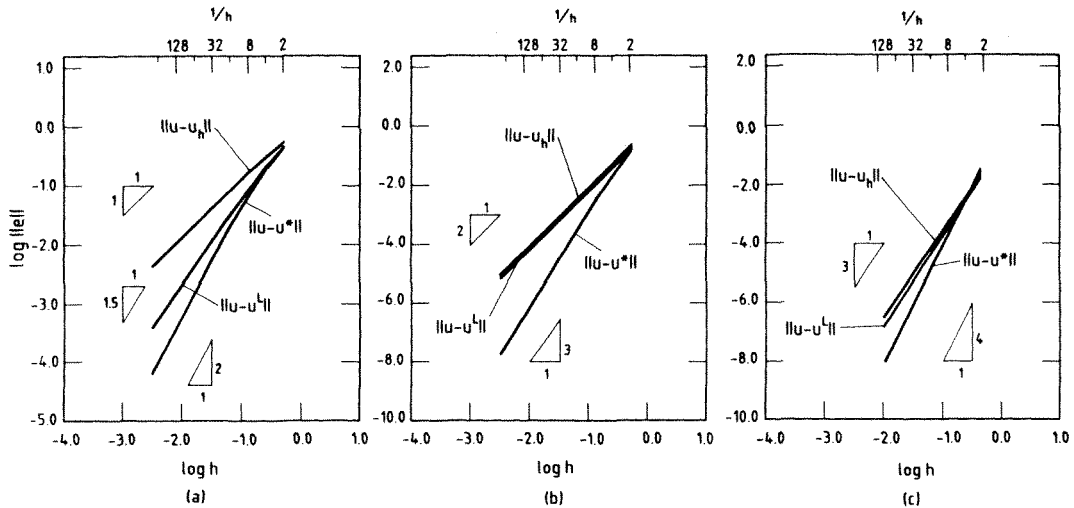
Figure 15. Rate of convergence of finite element and recovered solutions in energy norm. Problem of Example 1: (a) Linear element; (b) Quadratic element; (c) Cubic element

boundary point nodal values. The global convergence rate of the recovered solution in the energy norm is therefore generally lower.

3.3.2. Numerical experiments for two dimensional elements. In Figures 16(a)–16(e) we show the convergence of the recovered solutions for two dimensional elements in the energy norm on regular meshes used previously for Example 2.
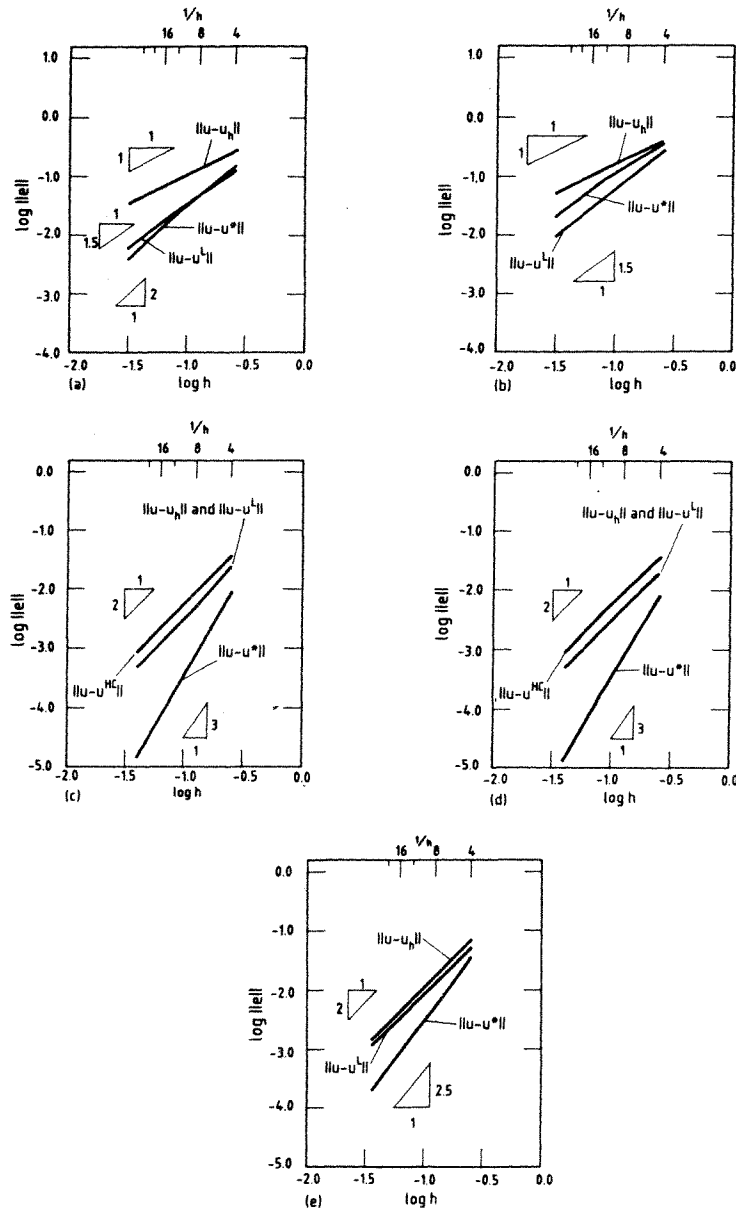
Figure 16. Rate of convergence of finite element and recovered solutions in energy norm. Two dimensional problem of Example 2: (a) Linear elements—4 node quadratic; (b) Linear elements—3 node triangle; (c) Quadratic elements—8 node quadratic; (d) Quadratic elements—9 node quadratic; (e) Quadratic elements—6 node triangle

Figures 16(a) and 16(b) show the results for linear 4 node quadrilateral and 3 node triangular elements. Figures 16(c), 16(d) and 16(e) present the results for quadratic 8 and 9 node quadrilaterals and 6 node triangles. These results are also demonstrated in Tables X(a)–X(e) respectively in the Appendix.
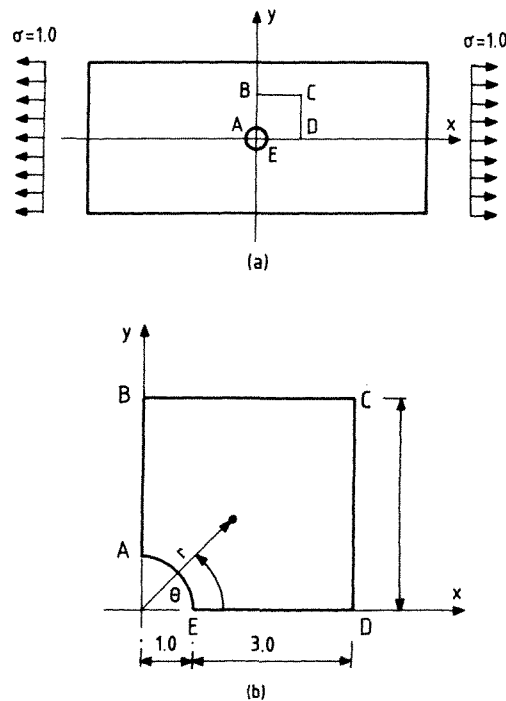
Figure 17. Infinite plate with a central circular hole subjected to unidirectional tensile loads: (a) The problem; (b) Portion of the plate analysed

Mesh 1   Mesh 2   Mesh 3
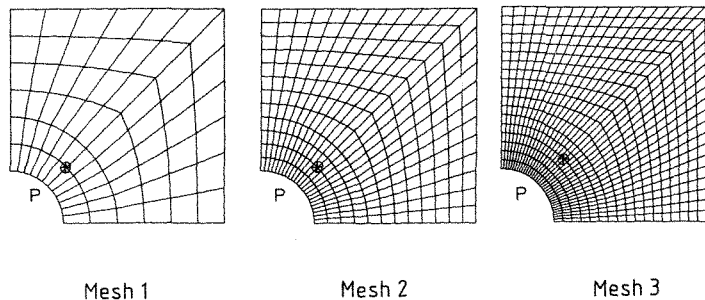
Figure 18. Meshes used in the analysis of the elastic problem. 'P' is the point for which convergence study is shown in Figure 19

For a 4 node quadrilateral element $\| e^* \|$ is superconvergent with a convergence rate of $O(h^2)$. For linear triangles, however, the convergence rate of $\| e^* \|$ is less than that expected and approximates to $O(h^{1.5})$. It is also observed that $\| e^L \|$ has a convergence rate of $O(h^{1.5})$ for both 4 and 3 node elements.

With quadratic elements the results of $\| e^* \|$ show $O(h^3)$ superconvergent behaviour for quadrilaterals with a slightly lower value of $O(h^{2.5})$ for triangles where boundary recovery computations are evidently less effective. An improved method for the implementation of the
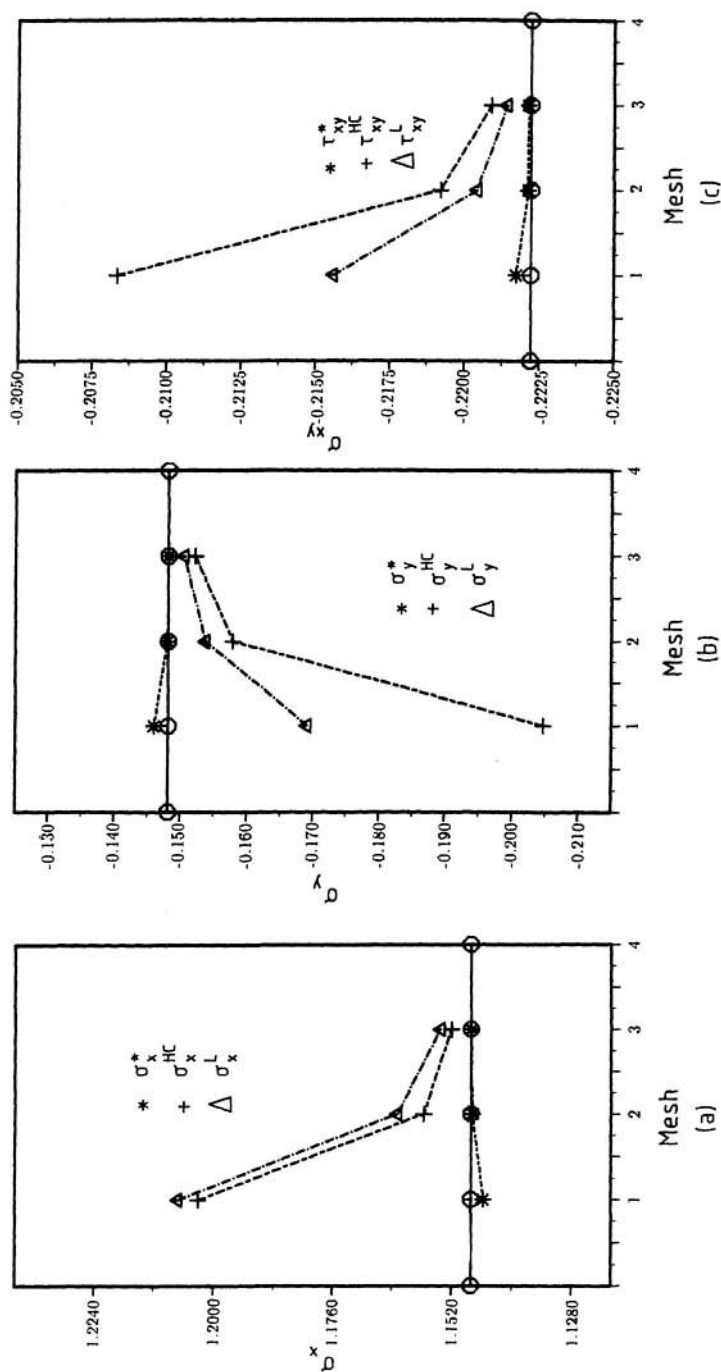
Figure 19. Convergence of the recovered solutions σ^L, σ^{HC} and σ^* at point 'P' for the elastic problem of Figure 18: (a) Convergence of σ_x^L, σ_x^{HC} and σ_x^*; (b) Convergence of σ_y^L, σ_y^{HC} and σ_y^*; (c) Convergence of τ_{xy}^L, τ_{xy}^{HC} and τ_{xy}^*

recovery technique in the boundary domain is now being investigated. However, all the results of recovered solution $\|e^*\|$ can still be considered as superconvergent. It is also observed that the results provided by $\|e^L\|$ and $\|e^{HC}\|$ again have only a standard convergence rate.

3.4. The convergence of the recovered nodal stresses for an elastic problem

Finally, we consider a problem of elasticity to demonstrate the accuracy of the recovered nodal stresses. For the sake of the length of the paper, here only the results of the recovery procedures for a 9 node quadrilateral element are reported. The performance of the recovery procedures for other elements is the same as we discussed in the previous sections.

Example 4. The problem considered is a portion of an infinite plate with a central circular hole subjected to unidirectional tensile loads $\sigma = 1\cdot0$ (see Figure 17(a)). The geometry of the problem is shown in Figure 17(b). Plane strain conditions are assumed with a Poisson's ratio of $0\cdot3$ and Young's modulus $E = 1000$. The boundary conditions are prescribed such that on edges AB and ED symmetry conditions are imposed and on edges BC and DC the plate is loaded by tractions given by an analytic solution expressed as

$$\sigma_x = 1 - \frac{a^2}{r^2}\left(\frac{3}{2}\cos 2\theta + \cos 4\theta\right) + \frac{3}{2}\frac{a^4}{r^4}\cos 4\theta$$

$$\sigma_y = -\frac{a^2}{r^2}\left(\frac{1}{2}\cos 2\theta - \cos 4\theta\right) - \frac{3}{2}\frac{a^4}{r^4}\cos 4\theta \tag{36}$$

$$\tau_{xy} = -\frac{a^2}{r^2}\left(\frac{1}{2}\sin 2\theta + \sin 4\theta\right) + \frac{3}{2}\frac{a^4}{r^4}\sin 4\theta$$

where (r, θ) are the usual polar co-ordinates.

Three meshes are used in the analysis shown in Figure 18. As the meshes are not fully regular, we shall examine the convergence of the recovered nodal stresses by directly comparing their values with the exact solution. The recovered stresses σ^L, σ^{HC} and σ^* are examined at a vertex nodal point with co-ordinates of $(1\cdot0606602, 1\cdot0606602)$ (or polar co-ordinates of $(1\cdot5, 45°)$) where the exact solution has the values of $\sigma_x = 1\cdot1481481$, $\sigma_y = -0\cdot14814810$ and $\tau_{xy} = -0\cdot22222229$.

The convergence of the recovered stress component of σ^L, σ^{HC} and σ^* are plotted in Figures 19(a), 19(b) and 19(c). It is observed that the results of σ^L and σ^{HC} are of similar accuracy. However, σ^* is much more accurate than σ^L and σ^{HC}. In fact, the values of each component of σ^* on the coarse mesh (mesh 1) are more accurate than the corresponding component values of σ^L and σ^{HC} on the fine mesh (mesh 3). The superiority of the proposed recovery technique over the global L_2 projection and Hinton–Campbell local extrapolation is clearly demonstrated. These results are also included in Tables XI(a), XI(b) and XI(c) in the Appendix.

4. CONCLUDING REMARKS

The superconvergent recovery technique prescribed in this paper is shown to yield higher accuracy than previously used methods which are frequently incorporated in existing codes. As its cost is small we recommend it strongly for practical post-processing of the results of finite element analysis to give enhanced accuracy.

In particular, the reader should note the very much improved nodal values for quadratic quadrilaterals over the Hinton–Campbell type of smoothing which previously was strongly recommended by the first author.[5]

Those using the versatile quadratic triangular element will doubtless be pleased to note the very high rate of convergence now applicable.

While only relatively simple one and two dimensional problems were here tested the procedure is applicable in an obvious manner to three dimensional analysis and indeed to problems such as plates and shells. Again, in three dimensional analysis we would expect an $O(h^4)$ rate of convergence for quadratic tetrahedra at internal nodes.

The reader should note that *superconvergence* of local values occurs with the new method for both interior and boundary nodes. However, the phenomenon of ultraconvergence, i.e. convergence at a rate $O(h^{p+2})$, is limited to internal nodes only. This will result in the energy norm error being only superconvergent with $O(h^{p+\alpha})$ ($\alpha \geqslant 1$ for one-D elements and two-D quadrilateral elements and $\alpha \geqslant 0.5$ for triangular elements) as in this norm the total domain is considered.

The full importance of the superconvergent recovery process will be discussed in the second part of the paper where error estimation is considered. Clearly the improved accuracy will serve to better determine the error magnitudes and to ensure narrow bounds of the effectivity index of the *a posteriori* error estimator.

APPENDIX

Detail of some numerical results

Table I(a). Example 1 of one dimensional problem. Derivatives σ_h, σ^L and σ^* of linear element evaluated at $x = 0.5$. Exact solution $\sigma(0.5) = 0.4485588705$

h	σ_h	σ^L	σ^*	$|\sigma - \sigma_h|$	$|\sigma - \sigma^L|$	$|\sigma - \sigma^*|$
1/2	-0.326743	0.000000	0.000000	0.7753(00)	0.4485(00)	0.4485(00)
1/4	0.319445	0.552067	0.368044	0.1291(00)	0.1035(00)	0.8051(-1)
1/8	0.418455	0.457010	0.430336	0.3010(-1)	0.8451(-2)	0.1822(-1)
1/16	0.439677	0.449920	0.444121	0.8882(-2)	0.1361(-2)	0.4437(-2)
1/32	0.445420	0.448896	0.447457	0.3139(-2)	0.3370(-3)	0.1102(-2)
1/64	0.447288	0.448643	0.448284	0.1270(-2)	0.8416(-4)	0.2750(-3)
1/128	0.447995	0.448580	0.448490	0.5635(-3)	0.2103(-4)	0.6873(-4)
1/256	0.448295	0.448564	0.448542	0.2642(-3)	0.5258(-5)	0.1718(-4)
Rate of convergence				1	2	2

Table I(b). Example 1 of one dimensional problem. Derivatives σ_h, σ^L and σ^* of quadratic element evaluated at $x = 0.5$. Exact solution $\sigma(0.5) = 0.4485588705$

h	σ_h	σ^L	σ^*	$|\sigma - \sigma_h|$	$|\sigma - \sigma^L|$	$|\sigma - \sigma^*|$
1/2	0.979991	0.758354	0.505570	0.5314(00)	0.3098(00)	0.5701(-1)
1/4	0.525239	0.511319	0.451893	0.7668(-1)	0.6276(-1)	0.3334(-2)
1/8	0.463302	0.461277	0.448764	0.1474(-1)	0.1272(-1)	0.2054(-3)
1/16	0.451806	0.451505	0.448572	0.3247(-2)	0.2946.(-2)	0.1279(-4)
1/32	0.449322	0.449281	0.448560	0.7630(-3)	0.7226(-3)	0.7989(-6)
1/64	0.448744	0.448739	0.448559	0.1850(-3)	0.1798(-3)	0.4992(-7)
1/128	0.448604	0.448604	0.448559	0.4556(-4)	0.4489(-4)	0.3119(-8)
Rate of convergence				2	2	4

Table I(c). Example 1 of one dimensional problem. Derivatives σ_h, σ^L and σ^* of cubic element evaluated at $x = 0.5$. Exact solution $\sigma(0.5) = 0.4485588705$

h	σ_h	σ^L	σ^*	$|\sigma - \sigma_h|$	$|\sigma - \sigma^L|$	$|\sigma - \sigma^*|$
1/2	0.345502	0.403163	0.477337	0.1031(00)	0.4540(-1)	0.2878(-1)
1/4	0.441073	0.447678	0.450154	0.7486(-2)	0.8810(-3)	0.1595(-2)
1/8	0.447840	0.448475	0.448656	0.7186(-3)	0.8428(-4)	0.9672(-4)
1/16	0.448480	0.448553	0.448565	0.7882(-4)	0.5369(-5)	0.5599(-5)
1/32	0.448550	0.448558	0.448559	0.9232(-5)	0.3363(-6)	0.3742(-6)
1/64	0.448558	0.448559	0.448559	0.1117(-5)	0.2103(-7)	0.2338(-7)
Rate of convergence				3	4	4

Table II. Derivatives σ_x^L and σ_x^* of 4 node element at $(0.25, 0.25)$. $u = x(1 - x)y(1 - y)(1 + 2x + 7y)$. Exact solution $\sigma_x = 0.375$. 4 term smoothing. Example 2

h	σ_x^L	σ_x^*	$|\sigma_x - \sigma_x^L|$	$|\sigma_x - \sigma_x^*|$
1/4	0.39101454	0.36375288	0.16014536(-1)	0.11247120(-1)
1/8	0.37894798	0.37164927	0.39479809(-2)	0.33507392(-2)
1/12	0.37697945	0.37346317	0.19794507(-2)	0.15368350(-2)
1/16	0.37606955	0.37412605	0.10695531(-2)	0.87394724(-3)
1/20	0.37568440	0.37443793	0.68439994(-3)	0.56206790(-3)
1/24	0.37547582	0.37460851	0.47582263(-3)	0.39149499(-3)
1/28	0.37534928	0.37471217	0.34927940(-3)	0.28782938(-3)
Rate of convergence			2	2

Table III. Derivatives σ_x^{HC} and σ_x^* of 8 node element at (0·25, 0·25). $u = x(1 - x)y(1 - y)(1 + 2x + 7y)$. Exact solution $\sigma_x = 0.375$. 8 term smoothing. Example 2

h	σ_x^{HC}	σ_x^*	$\mid \sigma_x - \sigma_x^{HC} \mid$	$\mid \sigma_x - \sigma_x^* \mid$
1/4	0.38997235	0.37203059	0.14972353(-1)	0.29694134(-2)
1/8	0.37861427	0.37484293	0.36142662(-2)	0.15706739(-3)
1/12	0.37659930	0.37496750	0.15992983(-2)	0.32503086(-4)
1/16	0.37589770	0.37498983	0.89770264(-3)	0.10172337(-4)
1/20	0.37557396	0.37499583	0.57395676(-3)	0.41704743(-5)
Rate of convergence			2	4

Table IV. Derivatives σ_x^{HC}, σ_x^L and σ_x^* of 9 node element at (0·25, 0·25). $u = x(1 - x)y(1 - y)(1 + 2x + 7y)$. Exact solution $\sigma_x = 0.375$. 8 term smoothing. Example 2

h	σ_x^{HC}	σ^L	σ^*	$\mid \sigma_x - \sigma^{HC} \mid$	$\mid \sigma_x - \sigma^L \mid$	$\mid \sigma_x - \sigma^* \mid$
1/4	0.38997	0.38684	0.37239	0.14974(-1)	0.11836(-1)	0.26042(-2)
1/8	0.37862	0.37794	0.37484	0.36214(-2)	0.29391(-2)	0.16276(-3)
1/12	0.37660	0.37630	0.37497	0.15991(-2)	0.13038(-2)	0.32281(-4)
1/16	0.37590	0.37573	0.37499	0.89772(-3)	0.73347(-3)	0.10172(-4)
1/20	0.37557	0.37547	0.37499	0.57396(-3)	0.46939(-3)	0.41667(-5)
Rate of convergence				2	2	4

Table V. Derivatives σ_x^L and σ_x^* of 3 node element at (0·25, 0·25). $u = x(1 - x)y(1 - y)(1 + 2x + 7y)$. Exact solution $\sigma_x = 0.375$. 3 term smoothing. Example 2

h	σ_x^L	σ_x^*	$\mid \sigma_x - \sigma_x^L \mid$	$\mid \sigma_x - \sigma_x^* \mid$
1/4	0.30658243	0.28964120	0.68417568(-1)	0.85358796(-1)
1/8	0.37406096	0.34995407	0.93904105(-3)	0.25045930(-1)
1/12	0.37102195	0.36349963	0.39780527(-2)	0.11500367(-1)
1/16	0.37352006	0.36845526	0.14799427(-2)	0.65447375(-2)
1/20	0.37389216	0.37078886	0.11078399(-2)	0.42111375(-2)
1/24	0.37425969	0.37206646	0.74030670(-3)	0.29335448(-2)
1/28	0.37445295	0.37284207	0.54705134(-3)	0.21579325(-2)
Rate of convergence			2	2

Table VI. Derivatives σ_x^L and σ_x^* of 6 node element at (0·25, 0·25). $u = x(1 - x)y(1 - y)(1 + 2x + 7y)$. Exact solution $\sigma_x = 0\cdot375$. 6 term smoothing. Example 2

h	σ_x^L	$\sigma_x^\bullet$	$\mid \sigma_x - \sigma_x^L \mid$	$\mid \sigma_x - \sigma_x^* \mid$
1/4	0.40600284	0.37084961	0.31002835(-1)	0.41503906(-2)
1/8	0.38387940	0.37474060	0.88793961(-2)	0.25939941(-3)
1/12	0.37914812	0.37494929	0.41481154(-2)	0.50710886(-4)
1/16	0.37739385	0.37498379	0.23938539(-2)	0.16212463(-4)
1/20	0.37655176	0.37499336	0.15517583(-2)	0.66406250(-5)
Rate of convergence			2	4

Table VII. Derivative σ_x^* of 12 node element at (0·75, 0·75). $u = 1 + xy + sh(4x + 4y)$. Exact solution $\sigma_x = 0\cdot80761254(+3)$. 13 term smoothing. Example 3

h	$\sigma_x^\bullet$	$\mid \sigma_x - \sigma_x^* \mid$
1/4	0.80267526(+3)	0.49372832(+1)
1/8	0.80729500(+3)	0.31754326(00)
1/12	0.80755897(+3)	0.53577066(-1)
1/16	0.80759503(+3)	0.17517144(-1)
1/20	0.80760575(+3)	0.67925664(-2)
Rate of convergence		4

Table VIII. Derivative σ_x^* of 16 node element at (0·75, 0·75). $u = 1 + xy + sh(4x + 4y)$. Exact solution $\sigma_x = 0\cdot80761254(+3)$. 15 term smoothing. Example 3

h	$\sigma_x^\bullet$	$\mid \sigma_x - \sigma_x^* \mid$
1/4	0.80309398(+3)	0.45185664(+1)
1/8	0.80733859(+3)	0.27395504(00)
1/12	0.80755848(+3)	0.54060180(-1)
1/16	0.80759522(+3)	0.17322419(-1)
1/20	0.80760581(+3)	0.67346531(-2)
Rate of convergence		4

Table IX(a). The convergence of the finite element and recovered solutions in energy norm. Linear element. Example 1

h	$\| u - u_h \|$	$\| u - u^L \|$	$\| u - u^* \|$
1/2	0.51785524	0.45658607	0.45870926
1/4	0.30713108	0.20245500	0.19363333
1/8	0.16062095	0.83534230(-1)	0.67373268(-1)
1/16	0.81230194(-1)	0.31872458(-1)	0.20159544(-1)
1/32	0.40731294(-1)	0.11691758(-1)	0.55322114(-2)
1/64	0.20380210(-1)	0.42088527(-2)	0.14502025(-2)
1/128	0.10191927(-1)	0.15013567(-2)	0.37132130(-3)
1/256	0.50961912(-2)	0.53316113(-3)	0.93951098(-4)
Rate of convergence	1	1.5	2

Table IX(b). The convergence of the finite element and recovered solutions in energy norm. Quadratic element. Example 1

h	$\| u - u_h \|$	$\| u - u^L \|$	$\| u - u^* \|$
1/2	0.17656663	0.15133511	0.14006796
1/4	0.50271032(-1)	0.45633947(-1)	0.21426007(-1)
1/8	0.13045455(-1)	0.12539418(-1)	0.29120554(-2)
1/16	0.32931809(-2)	0.32503669(-2)	0.32929486(-3)
1/32	0.82531701(-3)	0.82217136(-3)	0.34120076(-4)
1/64	0.20645614(-3)	0.20624224(-3)	0.34579099(-5)
1/128	0.51621975(-4)	0.51608016(-4)	0.35767218(-6)
1/256	0.12905990(-4)	0.12905098(-4)	0.38660090(-7)
Rate of convergence	2	2	3

Table IX(c). The convergence of the finite element and recovered solutions in energy norm. Cubic element. Example 1

h	$\| u - u_h \|$	$\| u - u^L \|$	$\| u - u^* \|$
1/2	0.28495479(-1)	0.23726884(-1)	0.34877661(-1)
1/4	0.41792552(-2)	0.32511614(-2)	0.29886089(-2)
1/8	0.54676749(-3)	0.38676500(-3)	0.21938730(-3)
1/16	0.69159372(-4)	0.44623915(-4)	0.13883663(-4)
1/32	0.86707819(-5)	0.52231801(-5)	0.83689374(-6)
1/64	0.10846594(-5)	0.62564108(-6)	0.51043629(-7)
Rate of convergence	3	3	4

Table X(a). The convergence of the finite element and recovered solutions in energy norm. 4 node element. Example 2

h	$\| u - u_h \|$	$\| u - u^L \|$	$\| u - u^* \|$
1/4	0.26748684	0.13453210	0.14355462
1/8	0.13332049	0.47116232(-1)	0.45909074(-1)
1/12	0.88823390(-1)	0.25687632(-1)	0.22387867(-1)
1/16	0.66602482(-1)	0.16717353(-1)	0.13216675(-1)
1/20	0.53276361(-1)	0.11978947(-1)	0.87132015(-2)
1/24	0.44394437(-1)	0.91251136(-2)	0.61731586(-2)
Rate of convergence	1	1.5	2

Table X(b). The convergence of the finite element and recovered solutions in energy norm. 3 node element. Example 2

h	$\| u - u_h \|$	$\| u - u^L \|$	$\| u - u^* \|$
1/4	0.38790645	0.25492357	0.36272582
1/8	0.20030374	0.85631472(-1)	0.15067504
1/12	0.13438453	0.44629460(-1)	0.85642332(-1)
1/16	0.10101538	0.28180292(-1)	0.56752281(-1)
1/20	0.80896844(-1)	0.19776118(-1)	0.41081802(-1)
1/24	0.67452504(-1)	0.14836369(-1)	0.30994459(-1)
Rate of convergence	1	1.5	1.5

Table X(c). The convergence of the finite element and recovered solutions in energy norm.
8 node element. Example 2

h	$\| u - u_h \|$	$\| u - u^L \|$	$\| u - u^{HC} \|$	$\| u - u^* \|$
1/4	0.22064704(-1)	0.21900284(-1)	0.33413075(-1)	0.85819423(-2)
1/8	0.48199452(-2)	0.47716983(-2)	0.83717374(-2)	0.70366916(-3)
1/12	0.20970727(-2)	0.20836826(-2)	0.37272928(-2)	0.17326585(-3)
1/16	0.11701710(-2)	0.11654598(-2)	0.20971616(-2)	0.65316723(-4)
1/20	0.74663122(-3)	0.74454996(-3)	0.13425662(-2)	0.30880041(-4)
Rate of convergence	2	2	2	3

Table X(d). The convergence of the finite element and recovered solutions in energy norm.
9 node element. Example 2

h	$\| u - u_h \|$	$\| u - u^L \|$	$\| u - u^{HC} \|$	$\| u - u^* \|$
1/4	0.18713278(-1)	0.18712126(-1)	0.33116702(-1)	0.79634889(-2)
1/8	0.46525246(-2)	0.46524580(-2)	0.83667226(-2)	0.69147166(-3)
1/12	0.20676849(-2)	0.20676817(-2)	0.37268371(-2)	0.17203745(-3)
1/16	0.11615134(-2)	0.11615407(-2)	0.20970799(-2)	0.65076879(-4)
1/20	0.74324421(-3)	0.74326613(-3)	0.13425445(-2)	0.30811753(-4)
Rate of convergence	2	2	2	3

Table X(e). The convergence of the finite element and recovered solutions in
energy norm. 6 node element. Example 2

h	$\| u - u_h \|$	$\| u - u^L \|$	$\| u - u^* \|$
1/4	0.67077312(-1)	0.49236800(-1)	0.32368422(-1)
1/8	0.17189408(-1)	0.13134771(-1)	0.51779855(-2)
1/12	0.76766102(-2)	0.59324074(-2)	0.19432675(-2)
1/16	0.43237537(-2)	0.33566279(-2)	0.89165488(-3)
1/20	0.27692325(-2)	0.21547584(-2)	0.51268938(-3)
Rate of convergence	2	2	2.5

Table XI(a). Example 4 of elastic problem. Derivatives σ_x^L, σ_x^{HC} and σ_x^* of 9 node element evaluated at (1·0606602, 1·0606602)

mesh	σ_x^L	σ_x^{HC}	σ_x^*
1	1.20709	1.20308	1.14567
2	1.26293	1.15762	1.14785
3	1.15423	1.15204	1.14802
Exact solution σ_x		1.1481481	

Table XI(b). Example 4 of elastic problem. Derivatives σ_y^L, σ_y^{HC} and σ_y^* of 9 node element evaluated at (1·0606602, 1·0606602)

mesh	σ_y^L	σ_y^{HC}	σ_y^*
1	-0.169072	-0.204736	-0.146020
2	-0.153742	-0.157871	-0.148020
3	-0.150563	-0.152217	-0.148199
Exact solution σ_y		-0.14814810	

Table XI(c). Example 4 of elastic problem. Derivatives σ_{xy}^L, σ_{xy}^{HC} and σ_{xy}^* of 9 node element evaluated at (1·0606602, 1·0606602)

mesh	σ_{xy}^L	σ_{xy}^{HC}	σ_{xy}^*
1	-0.215608	-0.208345	-0.221720
2	-0.220427	-0.219207	-0.222123
3	-0.221414	-0.220897	-0.222130
Exact solution σ_{xy}		-0.22222229	

REFERENCES

1. O. C. Zienkiewicz and J. Z. Zhu, 'A simple error estimator and adaptive procedure for practical engineering analysis', *Int. j. numer. methods eng.*, **24**, 337–357 (1987).
2. M. Ainsworth, J. Z. Zhu, A. W. Craig and O. C. Zienkiewicz, 'Analysis of the Zienkiewicz–Zhu *a posteriori* error estimator in the finite element method', *Int. j. numer. methods eng.*, **28**, 2161–2174 (1989).
3. J. Z. Zhu and O. C. Zienkiewicz, 'Superconvergence recovery technique and *a posteriori* error estimators', *Int. j. numer. methods eng.*, **30**, 1321–1339 (1990).
4. O. C. Zienkiewicz and J. Z. Zhu, 'Adaptivity and mesh generation', *Int. j. numer. methods eng.*, **32**, 783–810 (1991).
5. O. C . Zienkiewicz and R. L. Taylor, *The Finite Element Method*, 4th edn, *Vol. I*, McGraw-Hill, New York, 1989.
6. T. Moan, 'Orthogonal polynomials and "best" numerical integration formulas on a triangle', *ZAMM*, **54**, 501–508 (1974).
7. J. Barlow, 'Optimal stress location in finite element method', *Int. j. numer. methods eng.*, **10**, 243–251 (1976).
8. M. Zlamal, 'Superconvergence and reduced integration in the finite element method', *Math. Comp.*, **32**, 663–685 (1978).
9. P. Lesaint and M. Zlamal, 'Superconvergence of the gradient of finite element solutions', *RAIRO Anal. Numer.*, **13**, 139–166 (1979).
10. C. M. Chen, 'Superconvergence of finite element solutions and their derivatives', *Numer. Math. J. Chinese Univ.*, **3**, 118–125 (1981).
11. R. J. Mackinnon and G. F. Carey, 'Superconvergent derivatives: A Taylor series analysis', *Int. j. numer. methods eng.*, **28**, 489–509 (1989).
12. C. M. Chen, 'Optimal points of the stresses for triangular linear element', *Numer. Math. J. Chinese Univ.*, **2**, 12–20 (1980).
13. N. Levine, 'Stress sampling points for linear triangles in the finite element method', *Numer. Anal.*, **5**, 407–427 (1985).
14. Q. D. Zhu, 'Uniform superconvergence estimates of derivatives for the finite element method', *Numer. Math. J. Chinese Univ.*, **5**, 311–318 (1983).
15. A. B. Andreev and R. D. Lazarov, 'Superconvergence of the gradient for quadratic triangular finite elements', *Numer. Methods P.D.E.'s*, **4**, 15–32 (1986).
16. M. F. Wheeler and J. R. Whiteman, 'Superconvergent recovery of gradients on subdomains from piecewise linear element approximations', *Numer. Methods Partial Differential Equations*, **3**, 65–82 (1987).
17. E. Hinton and J. S. Campbell, 'Local and global smoothing of discontinuous finite element functions using a least square method', *Int. j. numer. methods eng.*, **8**, 461–480 (1974).
18. M. Krizek and P. Neittaanmaki, 'On superconvergence techniques', *Acta Appl. Math.*, **9**, 175–198 (1987).
19. J. T. Oden and H. J. Brauchli, 'On the calculation of consistent stress distributions in finite element applications', *Int. j. numer. methods eng.*, **3**, 317–325 (1971).
20. J. T. Oden and J. N. Reddy, 'Note on an approximate method for computing consistent conjugate stresses in elastic finite elements', *Int. j. numer. methods eng.*, **6**, 55–61 (1973).
21. O. C. Zienkiewicz, X.-K. Li and S. Nakazawa, 'Iterative solution of mixed problems and the stress recovery procedures', *Commun. appl. numer. methods*, **1**, 3–9 (1985).
22. I. Babuska and A. Miller, 'The post-processing approach in the finite element method—Part I: Calculation of displacement, stresses, and other higher derivatives of the displacements', *Int. j. numer. methods eng.*, **20**, 1085–1109 (1984).
23. J. H. Bramble and A. H. Schatz, 'Higher order local accuracy by averaging in the finite element method', *Math. Comp.*, **31**, 94–111 (1977).
24. V. Thomee, 'High order local approximations to derivatives in the finite element method', *Math. Comp.*, **31**, 652–660 (1977).